PROCEEDINGS OF THE ROYAL SOCIETY B

rspb.royalsocietypublishing.org

Research

Cite this article: Fusco G, Hong PS, Hughes NC. 2014 Positional specification in the segmental growth pattern of an early arthropod. *Proc. R. Soc. B* **281**: 20133037.
http://dx.doi.org/10.1098/rspb.2013.3037

Received: 20 November 2013
Accepted: 23 January 2014

Subject Areas:
palaeontology, evolution, developmental biology

Keywords:
allometry, growth gradient, growth control, morphogen, trilobites

Author for correspondence:
Nigel C. Hughes
e-mail: nigel.hughes@ucr.edu

Electronic supplementary material is available at http://dx.doi.org/10.1098/rspb.2013.3037 or via http://rspb.royalsocietypublishing.org.

Royal Society Publishing

Positional specification in the segmental growth pattern of an early arthropod

Giuseppe Fusco[1], Paul S. Hong[2] and Nigel C. Hughes[3]

[1]Department of Biology, University of Padova, Padova 35131, Italy
[2]School of Earth and Environmental Sciences, Seoul National University, 151747 Seoul, Korea
[3]Department of Earth Sciences, University of California, Riverside, CA 92521, USA

In many arthropods, there is a change in relative segment size during post-embryonic development, but how segment differential growth is produced is little known. A new dataset of the highest quality specimens of the 429 Myr old trilobite *Aulacopleura koninckii* provides an unparalleled opportunity to investigate segment growth dynamics and its control in an early arthropod. Morphometric analysis across nine post-embryonic stages revealed a growth gradient in the trunk of *A. koninckii*. We contrastively tested different growth models referable to two distinct hypotheses of growth control for the developing trunk: (i) a segment-specific control, with individual segments having differential autonomous growth progression, and (ii) a regional control, with segment growth depending on their relative position along the main axis. We show that the trunk growth pattern of *A. koninckii* was consistent with a regional growth control producing a continuous growth gradient that was stable across all developmental stages investigated. The specific posterior-to-anterior decaying shape of the growth gradient suggests it deriving from the linear transduction of a graded signal, similar to those commonly provided by morphogens. A growth control depending on a form of positional specification, possibly realized through the linear interpretation of a graded signal, may represent the primitive condition for arthropod differential growth along the main body axis, from which the diverse and generally more complex forms of growth control in subsequent arthropods have evolved.

1. Introduction

A growth gradient is a distribution, along a body axis, of differential growth rates for serially arranged structures or sections of a structure [1]. In arthropods, growth gradients have been reported for limb articles, for trunk sclerites and for the series of appendages along the trunk [2,3]. However, although the relative size of body parts is a major trait in animal body organization, the underlying developmental mechanisms producing characteristic proportions are largely unknown [4]. Segmental growth patterns can result from different forms of growth control, whose elucidation is an essential step in the study of arthropod body plan development and evolution [5,6].

A concentration of well-preserved exoskeletons of the 429 Myr old trilobite *Aulacopleura koninckii* (figure 1) provides an unparalleled opportunity to explore post-embryonic development and its control in an early arthropod [7]. Here, we exploit a new dataset of the highest quality specimens that contains accurate measurements of individual segment length for much of the ontogeny of this species. The study is based on nine juvenile developmental stages, each marked by a moult (figure 2*a*), from stage D9 (with nine thoracic segments (TSs)) to stage D17 (with 17 TSs). During this developmental interval, at each moult a new segment appeared near the rear of a posterior trunk region with dorsally conjoined segments, the pygidium. Simultaneously, the anteriormost pygidial segment was added (released) into the thorax by the formation of a new articulation. The thorax comprised fully articulated segments [8,9] (see [10] for an outline of trilobite ontogeny and [7] for details of *A. koninckii* segmentation mode).

Morphometric analysis reveals a growth gradient in the trunk of *A. koninckii*. Both absolute axial growth rates (per-moult growth rates) and relative axial

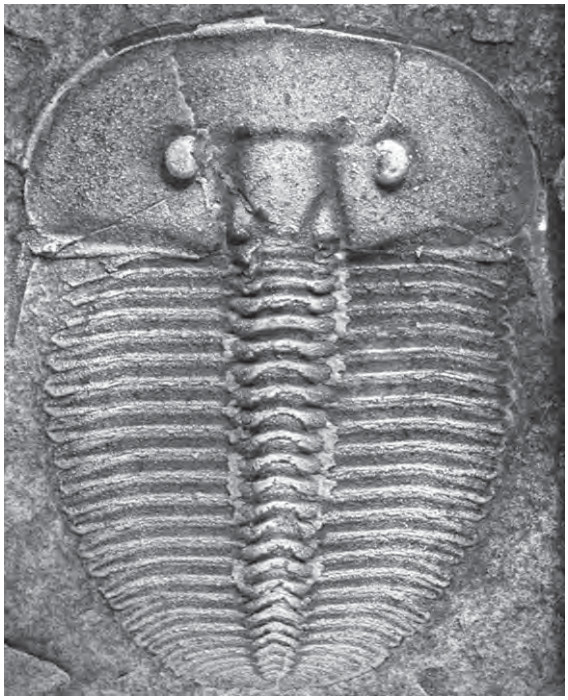

Figure 1. The 429 Myr old trilobite *A. koninckii*. Mature specimen with 19 TSs. Body length 11.7 mm.

growth rates (allometric coefficients with respect to trunk size) of TSs, as delimited by dorsal sclerite borders, exhibit declining values from posterior to anterior (figure 2*b*,*c*; electronic supplementary material, figure S1). The gradient evidently does not continue decaying to the front of the more anterior body region, the cephalon, because cephalic length has an average per-moult growth rate ($\pm$s.e.m.), which is significantly higher than that of the first TS, 1.087 ± 0.004 versus 1.058 ± 0.006 (one-tailed Student's *t*-test, $p = 0.0012$).

We considered two distinct hypotheses of growth control for the developing trunk throughout the interval of ontogeny studied. Under the *segmental gradient* (SG) *hypothesis*, the TSs represent early, individually specified growth fields and each segment, once released into the thorax, grew at a constant rate depending on its position in the sequence. The different values of growth rates of the segments determined the segmental gradient SG(i), a discrete function in the domain of natural numbers from 1 to 17 inclusive, where i is the ordinal position of a segment counting from the anterior to posterior (figure 3*a*,*b*). At some point in ontogeny, either at the time of the segment release into the thorax or before, the subsequent rate of growth of each segment was fixed, and trunk growth and segmental size composition of the thorax derived from the autonomous growth rates of the various segments. The SG hypothesis reflects the standard assumption that ontogenetic allometry results from differential constant growth rates of distinct body parts [11]. Under the *trunk gradient* (TG) *hypothesis*, the whole trunk was a growth field that exhibited a continuous steady growth gradient. Growth patterns of segments thus derived from the global growth pattern of the trunk. The different growth rates at each relative position along the trunk determined the scaling trunk gradient TG(x), a continuous function in the domain of real numbers from 0 to 1 inclusive, where x is the relative position of a point along the trunk, from the anterior to posterior (figure 3*c*,*d*). During ontogeny, individual segments changed their relative position (an interval of x-values) along the trunk, as a result of the differential growth of the various sections of the trunk. Accordingly, as they were subjected to different values of the gradient, their growth rates changed as well. Segment growth under the TG hypothesis involves a form of positional specification along the main body axis, i.e. the regulation of tissues' activity (in this case, axial growth) according to their positional values within a developing field [12].

The two competing growth control hypotheses were contrastively tested, comparing the predictions of different growth models for each hypothesis with observed segment size data across ontogeny.

2. Material and methods

(a) Specimen collection

Specimens of the aulacopleuride trilobite *A. koninckii* were collected from a 1.4 m thick interval of mudstone at a single locality on the northwest facing slope of Na Černidlech, near Loděnice, about 20 km west of Prague in the Czech Republic [13]. The interval includes numerous bedding planes, most of which contain articulated (i.e. complete) specimens of *A. koninckii* and is Middle Silurian in age. Specimens were preserved by multiple, apparently short-lived events of mudstone deposition of which there were over an hundred within the 1.4 m interval, which in total is estimated to represent the accumulation product of approximately 1000–10 000 years [14]. *Aulacopleura koninckii* specimens occur in dense concentrations on particular bedding planes and the outcrop was completely exploited by collectors in the early to mid-1800s. These collections were dispersed to museums worldwide but principal holdings are in the National Museum in Prague, the Czech Geological Survey and the Museum of Comparative Zoology at Harvard University.

(b) Specimen selection and data acquisition

The juvenile specimens studied herein belong to the so-called *meraspid* phase of development which, in this trilobite, was characterized by both the appearance of new trunk segments in a subterminal zone and the development of new articulations between existing segments. Morphometric data that are of cross-sectional type [15] (i.e. which allow stage assignment on the basis of a criterion independent of size, in this case, the number of TSs) can be obtained for the meraspid period only. From over 10 000 juvenile and mature articulated specimens inspected, 352 were selected that showed the most minimal evidence of postmortem distortion of original form, of which 137 are the meraspid specimens from stage D9 to D17 analysed in this study [16]. These are distributed as follows: 8 D9, 12 D10, 16 D11, 15 D12, 17 D13, 21 D14, 19 D15, 15 D16 and 14 D17.

The fossils were coated with ammonium chloride sublimate and photographed directly with a Nikon D100 digital camera and macrolens, through a Nikon SMZ-U stereomicroscope with a Nikon CoolPix995 digital camera or with a Leica MZ16 stereomicroscope with a Leica DFC420 digital camera. The resulting images where digitized using the NIH ImageJ software package (http://imagej.nih.gov/ij/) [17], with the x- and y-coordinates recorded for each of a series of marker points on each specimen. A scale in half-millimetre divisions was included in each image.

(c) Measurements

To obtain data on trunk segment length, a line along the sagittal axis was constructed on the image of each specimen. A line was then placed transversely to this, linking the articulating processes at the fulcral boss (the point abaxially marginal to the fulcrum). The intersection of this line and the sagittal axis was used to

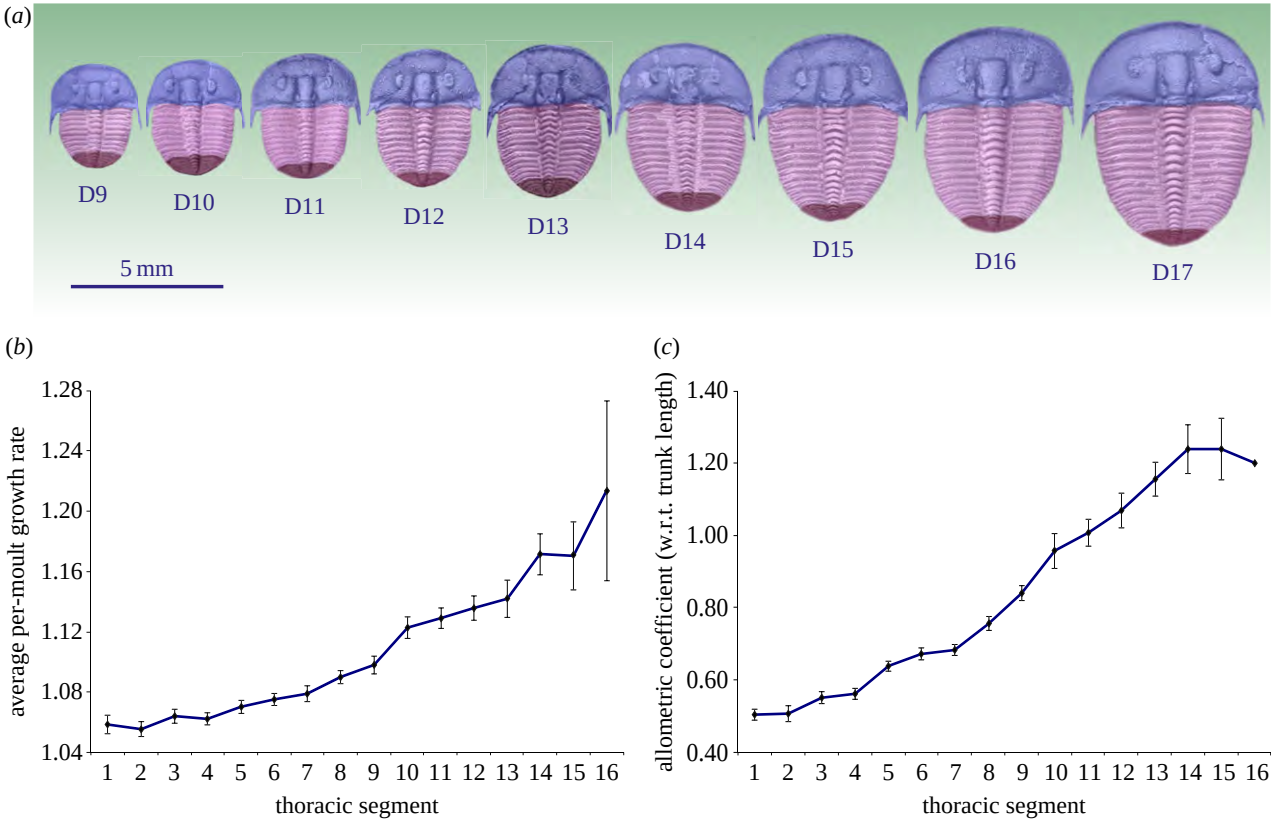

Figure 2. Growth gradient in the trunk of *A. koninckii*. (*a*) Schematic of the section of ontogeny considered: from developmental stage 9 (D9), with nine TSs, to developmental stage 17 (D17), with 17 TSs. Figured exemplars are scaled to the average size of each stage. Different colours indicate the main body regions: cephalon (blue), thorax (pink) and pygidium (purple). Thorax plus pygidium together constitute the trunk. TS per-moult growth rates (*b*) and TS ontogenetic allometric coefficients with respect to trunk length (*c*) both exhibit significant declining value from posterior to anterior (Spearman's rank correlation test, for both, $\rho = 0.991$, $p = 0.0001$, $n = 16$). TS11 grows approximately isometrically with regard to trunk length, while more anterior and more posterior segments show negative and positive allometry, respectively. Bars are standard errors (not calculable for TS16 in *c*), $n = 9$ for TS1–TS9 and decreases from $n = 8$ for TS10 to $n = 2$ for TS16.

represent the anterior of each segment and its *x*- and *y*-coordinates were recorded (electronic supplementary material, figure S2). Linear distances between landmarks were calibrated with the scale bar.

As longitudinal data, i.e. data referring to an individual specimen's growth progression [15] are not available, growth data can only be based on average measures at each stage (see the electronic supplementary material). The dataset used to explore growth progression of TSs is composed of average measures for all segments and developmental stages in the ontogenetic interval D9–D17. This comprises 117 independent data ($n = 9$ for TS1–TS9 and decreases from 8 to 1 from TS10 to TS17). Mean standard errors can be calculated only for TS1–TS16.

(d) Growth gradient detection

The average per-moult growth rate (AGR_i) of the length of each TS *i* was calculated as the antilogarithm of the average per-moult growth increment (AGI_i) for the natural logarithmic transformation of the original variables at each stage *d*, ($LTS_{i,d}$, see the electronic supplementary material). AGI_i is calculated as the arithmetic mean of the increments in $\ln(LTS_{i,d})$ between pairs of contiguous stages in the ontogenetic series. AGR_i thus corresponds to the geometric mean of untransformed size values [10]. The AGR of cephalic length was calculated in the same way.

The ontogenetic allometric coefficients of each TS were calculated as the linear regression slope of $\ln(LTS_{i,d})$ versus $\ln(TRL_d)$ ($n = 9$ for TS1–TS9, n decreases from $n = 8$ for TS10 to $n = 2$ for TS16). The use of averages, rather than specimen data, is justified by the need to control for the bias of static (within stage) allometry, which can be quite substantial for the segments that are represented by only short spans of ontogeny, because they were released into the thorax at stages later than D9.

(e) Model comparison data

Although, in principle, the two competing hypotheses have clearly distinct expectations for the growth pattern of TSs, namely a constant rate under the SG hypothesis and a decreasing rate under the TG hypothesis, in practice a comparison cannot be directly performed on the basis of model fitting to observed segment growth rates. This is owing to two contingencies whose effects combine negatively. Firstly, the curvature of growth progression predicted by TG hypothesis is quite subtle, as in the D9–D17 section of meraspid ontogeny anterior segments changed their position (and thus growth rates) minimally, whereas posterior segments, which were released into the thorax at stages later than D9, have relatively short ontogenies (and thus growth rate variation). Secondly, per-stage observed segment growth rates are highly scattered, because each value is the ratio between the observed size values of two subsequent stages, which are extremely sensitive to sample errors (electronic supplementary material, figure S3). As an alternative, segment relative size measures are less sensitive to the sample error; thus predictions of the two hypotheses were compared using this dataset.

(f) Fitting functions

Nonlinear least-squares regression procedure was performed with the software STATGRAPHICS CENTURION v. XVI, using Marquardt's algorithm, as an estimation method. Details on fitting

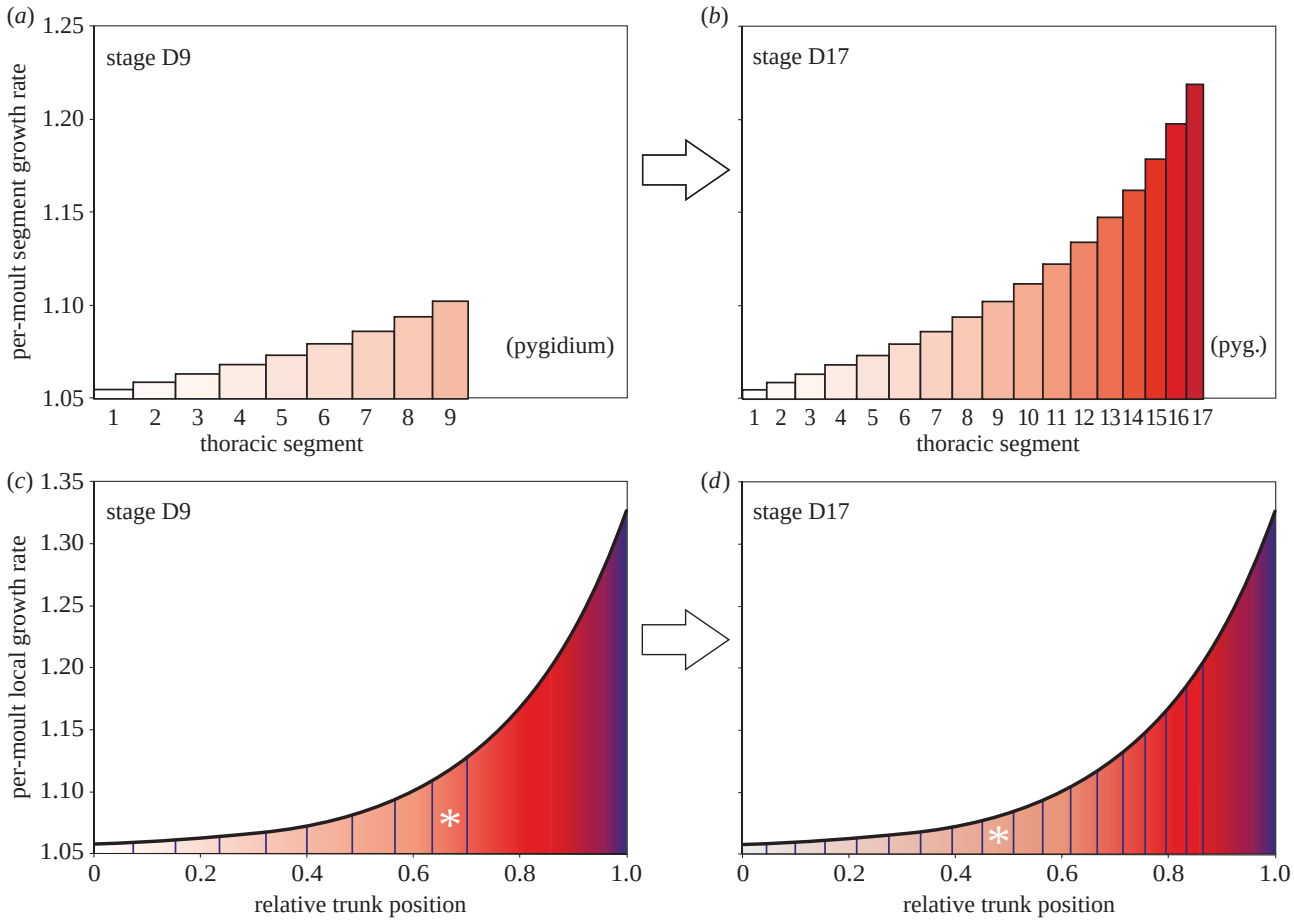

Figure 3. Schematic of the two growth control hypotheses under test. (*a*,*b*) *Segmental gradient* (SG) *hypothesis*. (*c*,*d*) *Trunk gradient* (TG) *hypothesis*. Left panel graphs (*a*,*c*) refer to the growth pattern at developmental stage D9 (with nine TSs); right panel graphs (*b*,*d*) refer to the growth pattern eight stages later, at stage D17 (with 17 TSs). Histogram bar widths in (*a*,*b*) and the space between vertical blue lines in (*c*,*d*) indicate the length of TSs on the basis of the observed data. Under the SG hypothesis, once segments were released into the thorax, they grew at a constant per-moult growth rate. The specific constant growth rate of each segment produced a decaying growth gradient from the posterior forwards. Under the TG hypothesis, the trunk as a whole exhibited a steady, decaying growth gradient. Growth patterns of individual segments were thus derived from the global growth pattern of the trunk. The difference between the two growth control hypotheses is not in the contrast between a continuous and a stepwise distribution of growth rates, but rather that in the SG hypothesis growth rate was segment-specific, while in the TG hypothesis each segment experienced a growth rate that depended on its relative position along the trunk, and this varied (declined) with ontogeny. See, for instance, the different relative position of TS9 (marked with a star) at stage D9 and D17 under TG hypothesis, with the consequent change in the growth rate.

function derivation and fitting procedure implementation are given in the electronic supplementary material.

3. Results

Different growth gradient functions can be modelled under each of the two hypotheses; thus in order to contrastively test the latter, we screened several functions for each hypothesis through least-squares regression on observed data. We show here the comparison between the two best-performing models for each hypothesis. The SG models are a geometric progression ($\mathrm{SGgmp}(i) = a + be^{wi}$) and a power progression ($\mathrm{SGpwp}(i) = a + bi^{w}$), while the TG models are an exponential function ($\mathrm{TGexp}(x) = a + be^{-w(1-x)}$) and a power-law function ($\mathrm{TGpwl}(x) = a + b(1 - x + c)^{-w}$). TGexp and TGpwl functions actually have two and three parameters, respectively, as in both formulae the parameter a can be expressed in terms of the remaining parameters (see the electronic supplementary material). The four models have very different structures and none is nested within any other; thus they have been compared with each other using the corrected Akaike Information Criterion ($\mathrm{AIC_c}$, table 1).

Both TG models exhibit normalized probabilities larger than 0.9999 of being the correct model when compared with either SG model, with evidential ratios (R) in the order of billions. Within each hypothesis, the SGpwp model is slightly better supported than the SGgmp model ($R = 1.60$), while the TGexp model has somewhat greater support than the TGpwl model ($R = 2.68$). The fit of the models to the data can be sensibly improved by eliminating a few outliers; however, as the outliers are not the same for SG and TG models, we have presented the result with the complete dataset, but taking out the outliers of all models does not change the results of the comparisons (electronic supplementary material, table S1). The SG models have consistently inferior fitting performances with respect to TG models and this is because they cannot account for the slight decrease in segment growth rate with ontogeny. Both TG models explain a substantial fraction of the observed variance in the growth pattern (for both $r^2 = 98.56\%$, $n = 100$; figure 4), but there is no strong evidence to favour one TG model over the other. The TGpwl model produces slightly smaller residuals, but the TGexp model has somewhat higher probability because of the smaller number or parameters of the latter. This result is consistent when the few TG outliers are

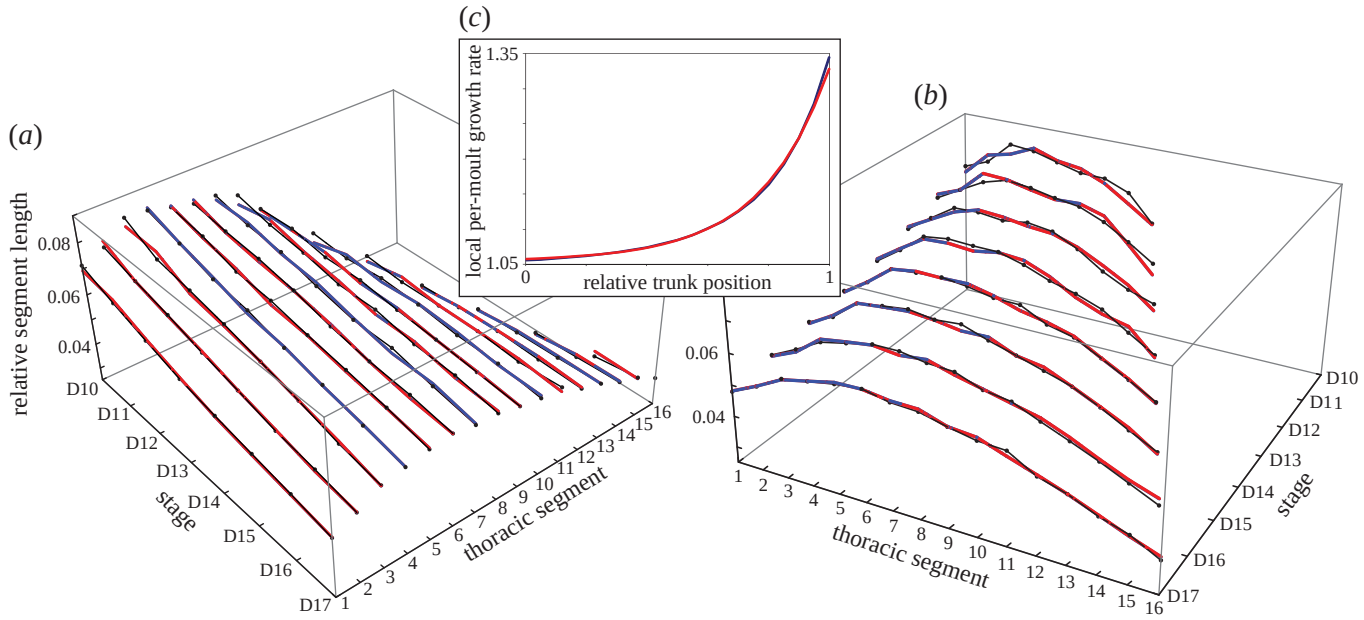

Figure 4. Fitting of the TGexp and TGpwl models to the observed distribution of relative TS lengths. (*a*) Lines show the changes in the relative length of each TS TS1–TS16 across the ontogenetic stages D10–D17. (*b*) Lines show the thoracic profile at each ontogenetic stage D10–D17, as represented by the relative lengths of its TSs. Black dots and lines, observed values; red lines TGexp calculated values, blue lines TGpwl calculated values. With this set of estimated parameter values (same as in table 1), the two growth gradients are largely overlapping (*c*), but see text.

Table 1. Results of AIC_c comparison for the four competing models to the dataset of relative TS lengths. no. par., number of estimated parameters; ΔAIC_c, difference in corrected Akaike score with respect to the model with the minimum score; $wAIC_c$, Akaike weight, the probability of being the correct model among the set of candidate models. The normalized probability for a model i of being the correct model with respect to a competing model j is $P = (wAIC_c)_i/[(wAIC_c)_i + (wAIC_c)_j]$. The strength of evidence in favour of one model (or a set of models) over a competing model (or a disjunct set of competing models), the evidential ratio, is the ratio between its Akaike weight (or the summation of the Akaike weights of the set of models) and the Akaike weight of the competing model (or the summation of the Akaike weights of the competing set). The evidential ratio of the two TG models versus the two SG models is 2.17×10^{10} and the evidential ratio of TGexp versus TGpwl is 2.68. The number of observations on which the calculation is based is 100.

model	no. par.	ΔAIC_c	$wAIC_c$
SGgmp	3	48.88	1.77×10^{-11}
SGpwp	3	47.94	2.83×10^{-11}
TGexp	2	0	0.729
TGpwl	3	1.97	0.271

eliminated (TGexp $r^2 = 98.97\%$, TGpwl $r^2 = 98.98\%$, $n = 96$; electronic supplementary material, table S2).

It is also possible to fit the two TG models to a related dataset which is more specific for the TG hypothesis, namely the set of relative positions of the boundaries between segments, simply considered as trunk landmarks, irrespectively of their relation to the corresponding segment (both models, $r^2 = 99.995\%$, $n = 96$; electronic supplementary material, figure S4). Here the TGpwl gains some support over the TGexp model ($R = 4.02$, $p = 0.801$), while at the same time the shape of the TGpwl gradient departs more markedly from that of TGexp (electronic supplementary material, table S3 and figure S5), but this does not resolve the matter decisively.

The inability of this analysis to choose between the two TG models with sufficient support is owing to the fact that the more marked differences between the two functions tend to emerge in the region of the trunk, approximately the most posterior 10th, for which there are no local growth data. Nonetheless, we can conclude with confidence that the trunk segments of *A. koninckii*, while morphologically individualized, were under a long-range growth control operating at the level of a more inclusive body region.

4. Discussion

The simple observation of an anterior-to-posterior graded distribution of segment growth rates in a given body region may suggest the existence of a segmental growth gradient, with each segment representing an autonomous growth field. However, only an accurate morphometric inspection of the growth pattern, like that implemented herein, can reveal whether this results from a different underlying growth process, based on another form of growth control. This is what we have found in *A. koninckii*, where the whole trunk was a growth field, and segments grew according to their relative position within the trunk. The possibility that the description of a growth gradient based on discrete body units might be only 'a crude representation of the true growth-gradient' was anticipated by J. Huxley himself ([1], p. 81), and here we provide a clear example of that.

The continuous steady-state scaling growth gradient detected in the trunk of *A. koninckii* implies that the observed differential segment growth was an epiphenomenon of the growth pattern of the whole trunk and did not depend on segment delimitation *per se*. In this respect, the boundaries of the dorsal sclerites of each TS can be seen as morphological landmarks on a continuous growth field, useful for morphometric analysis, but not as boundaries relevant to the growth process itself. Under this form of regional growth control, the way segment boundaries are specified and developed during

ontogeny, i.e. the species-specific segmentation mode [9], does not affect growth.

This form of growth control, based on long-range continuous positional specification, was likely implemented through a graded signal, whose nature obviously cannot be directly investigated in a fossil animal. However, the specific decaying shape of the regionally controlled trunk growth gradient of *A. koninckii* invites further considerations, in the light of extant organism studies on morphogen gradients and in the context of arthropod phylogeny. Morphogen gradients are thought to be a common way in which positional specification is implemented in extant organisms [18], where they play a fundamental role in pattern formation and growth [19]. In its most frequent usage, the term morphogen refers to a long-range signalling molecule that patterns a developing tissue in a concentration-dependent manner, instructing target cells to respond in specific ways, e.g. through cell differentiation or cell proliferation, depending on their location within a tissue [20,21]. Studies of morphogen dynamics in a variety of model organisms and organ systems show that different mechanisms of morphogen production, spreading and degradation can lead to steady-state morphogen gradients with distinct shapes, among which decaying exponential and power-law distributions are common approximations [22,23]. As stated above, our morphometric data cannot provide clues about the particular mechanism producing the putative graded signal that likely operated in the trunk of *A. koninckii*, as different mechanisms can produce the same pattern, especially in a system undergoing growth [24]. Nor can it yield insights into the specific response of the growing tissue, for instance involving the regulation of cell proliferation, in the form of a 'mitogenic gradient' [25]. However, it is worth noting an isomorphism between the shapes of the most common morphogen gradient distributions found by experiment in extant organisms (exponential and power-law) [26,27] and the shape of the growth gradient we found in the trunk of *A. koninckii*.

In general, a morphogen gradient need not correspond with a simple graded response in the target tissue, as the interpretation of the gradient can consist of complex nonlinear interactions between the signal and responding tissues [20]. However, if segment differential growth rate in *A. koninckii* was under the control of a morphogen signal, with effect, for instance, on the level of expression of some growth hormone receptors or of members of the signalling pathways downstream of them [5,28,29], as is likely when it is considered that genes and hormones involved in tissue growth are remarkably conserved in all animals [30], this signal was apparently transduced linearly into an isomorphic growth gradient response.

The precise phylogenetic position of trilobites within the arthropod clade is still in debate [31]. Nevertheless, irrespective of the actual basal branching topology of the arthropod phylogenetic tree, the relative short length (i.e. evolutionary time) of the branch connecting this ancient (429 Myr old) trilobite species to the basal node of the Arthropoda total group results in a sizeable probability for the state of its growth control characters representing the plesiomorphic condition [32–34]. A growth control depending on a form of positional specification along the main body axis, possibly realized through the linear transduction of a graded signal along the trunk into an isomorphic growth gradient, may thus represent the primitive condition for arthropod differential growth along the main body axis.

The study of mechanisms controlling growth and pattern formation is a topic of high interest in current research in developmental and evolutionary biology [35] and the data provided by this study are currently the oldest available window on axial growth control for a major bilaterian clade [10]. Exploration of departures from this pattern among other arthropods, living and fossil, offers the prospect of rich insight into the evolution of arthropod body patterning.

Acknowledgements. We thank D. E. G. Briggs, S. M. Hughes, G. Hunt, J. Jaeger and H. F. Nijhout for comments on a preliminary version of the article, P. Dai Pra and C. Romualdi for discussion on data analysis, R. Mazzaro and M. Simonetti for assistance with drawings, and P. Budil, J. Cundiff and V. Turek, for access to specimens.

Data accessibility. Morphometric raw measures are uploaded as electronic supplementary material.

Funding statement. This work was funded by NSF EAR-0616574.

References

1. Huxley JS. 1932 *Problems of relative growth*. London, UK: Methuen & Co.
2. Hartnoll RG. 1982 Growth. In *The biology of Crustacea*, vol. 2 (eds DE Bliss, LG Abele), pp. 111–196. New York, NY: Academic Press.
3. Heming BS. 2003 *Insect development and evolution*. Ithaca, NY: Comstock.
4. Nijhout HF, Grunert LW. 2010 The cellular and physiological mechanism of wing-body scaling in *Manduca sexta*. *Science* **330**, 1693–1695. (doi:10.1126/science.1197292)
5. Emlen DJ, Allen CE. 2003 Genotype to phenotype: physiological control of trait size and scaling in insects. *Integr. Comp. Biol.* **43**, 617–634. (doi:10.1093/icb/43.5.617)
6. Shingleton AW, Frankino WA, Flatt T, Nijhout HF, Emlen DJ. 2007 Size and shape: the developmental regulation of static allometry in insects. *BioEssays* **29**, 536–548. (doi:10.1002/bies.20584)
7. Fusco G, Hughes NC, Webster M, Minelli A. 2004 Exploring developmental modes in a fossil arthropod: growth and trunk segmentation of the trilobite *Aulacopleura konincki*. *Am. Nat.* **163**, 167–183. (doi:10.1086/381042)
8. Minelli A, Fusco G. 2013 Arthropod post-embryonic development. In *Arthropod biology and evolution. Molecules, development, morphology* (eds A Minelli, G Boxshall, G Fusco), pp. 91–122. Berlin, Germany: Springer.
9. Hughes NC, Minelli A, Fusco G. 2006 The ontogeny of trilobite segmentation: a comparative approach. *Paleobiology* **32**, 602–627. (doi:10.1666/06017.1)
10. Fusco G, Garland Jr T, Hunt G, Hughes NC. 2012 Developmental trait evolution in trilobites. *Evolution* **66**, 314–329. (doi:10.1111/j.1558-5646.2011.01447.x)
11. Nijhout HF. 2011 Dependence of morphometric allometries on the growth kinetics of body parts. *J. Theor. Biol.* **288**, 35–43. (doi:10.1016/j.jtbi.2011.08.008)
12. Wolpert L. 2011 Positional information and patterning revisited. *J. Theor. Biol.* **269**, 359–365. (doi:10.1016/j.jtbi.2010.10.034)
13. Hughes NC, Kříž J, MacQuaker JHS, Huff WD. In press. The depositional environment and taphonomy of the Homerian '*Aulacopleura* shales' fossil assemblage near Loděnice, Czech Republic (Prague Basin, Perunican microcontinent). *Bull. Geosci.*
14. Hughes NC, Chapman RE, Adrain JM. 1999 The stability of thoracic segmentation in trilobites: a case study in developmental and ecological constraints. *Evol. Dev.* **1**, 24–35. (doi:10.1046/j.1525-142x.1999.99005.x)
15. Cock AG. 1966 Genetical aspects of metrical growth and form in animals. *Q. Rev. Biol.* **41**, 131–190. (doi:10.1086/404940)

16. Hong PS, Hughes NC, Sheets HDS. In press. Size, shape, and systematics of the Silurian trilobite *Aulacopleura koninckii*. *J. Paleont*.
17. Abràmoff MD, Magalhães PJ, Ram SJ. 2004 Image processing with ImageJ. *Biophotonics International* **11**, 36–42.
18. Jaeger J, Irons D, Monk N. 2008 Regulative feedback in pattern formation: towards a general relativistic theory of positional information. *Development* **135**, 3175–3183. (doi:10.1242/dev.018697)
19. Schwank G, Basler K. 2010 Regulation of organ growth by morphogen gradients. *Cold Spring Harb. Perspect. Biol.* **2**, a001669. (doi:10.1101/cshperspect.a001669)
20. Rogers KW, Schier AF. 2011 Morphogen gradients: from generation to interpretation. *Annu. Rev. Cell Dev. Biol.* **27**, 377–407. (doi:10.1146/annurev-cellbio-092910-154148)
21. Ashe HL, Briscoe J. 2006 The interpretation of morphogen gradients. *Development* **133**, 385–394. (doi:10.1242/dev.02238)
22. Wartlick O, Kicheva A, González-Gaitán M. 2009 Morphogen gradient formation. *Cold Spring Harb. Perspect. Biol.* **1**, a001255. (doi:10.1101/cshperspect.a001255)
23. Barkai N, Shilo B-Z. 2009 Robust generation and decoding of morphogen gradients. *Cold Spring Harb. Perspect. Biol.* **1**, a001990. (doi:10.1101/cshperspect.a001990)
24. Chisholm RH, Hughes BD, Landman KA. 2010 Building a morphogen gradient without diffusion in a growing tissue. *PLoS ONE* **5**, e12857. (doi:10.1371/journal.pone.0012857)
25. Megason SG, McMahon AP. 2002 A mitogen gradient of dorsal midline Wnts organizes growth in the CNS. *Development* **129**, 2087–2098.
26. Grieneisen VA, Scheres B, Hogeweg P, Marée AFM. 2012 Morphogengineering roots: comparing mechanisms of morphogen gradient formation. *BMC Syst. Biol.* **6**, 37. (doi:10.1186/1752-0509-6-37)
27. Eldar A, Rosin D, Shilo BZ, Barkai N. 2003 Self-enhanced ligand degradation underlies robustness of morphogen gradients. *Dev. Cell.* **5**, 635–646. (doi:10.1016/S1534-5807(03)00292-2)
28. Tang HY, Smith-Caldas MSB, Driscoll MV, Salhadar S, Shingleton AW. 2011 FOXO regulates organ-specific phenotypic plasticity in *Drosophila*. *PLoS Genet.* **7**, e1002373. (doi:10.1371/journal.pgen.1002373)
29. Nijhout HF, Riddiford LM, Mirth C, Shingleton AW, Suzuki Y, Callier V. 2013 The developmental control of size in insects. *WIREs Dev. Biol.* **3**, 113–134. (doi:10.1002/wdev.124)
30. Shingleton AW. 2010 The regulation of organ size in *Drosophila*: physiology, plasticity, patterning and physical force. *Organogenesis* **6**, 76–87. (doi:10.4161/org.6.2.10375)
31. Edgecombe GD, Legg DA. 2013 The arthropod fossil record. In *Arthropod biology and evolution. Molecules, development, morphology* (eds A Minelli, G Boxshall, G Fusco), pp. 393–415. Berlin, Germany: Springer.
32. Donoghue MJ, Doyle JA, Gauthier J, Kluge AG, Rowe T. 1989 The importance of fossils in phylogeny reconstruction. *Ann. Rev. Ecol. Syst.* **20**, 431–460. (doi:10.1146/annurev.es.20.110189.002243)
33. Huelsenbeck JP. 1991 When are fossils better than extant taxa in phylogenetic analysis? *Syst. Zool.* **40**, 458–469. (doi:10.2307/2992240)
34. Harcourt-Brown KG, Pearson PN, Wilkinson M. 2001 The imbalance of paleontological trees. *Paleobiology* **27**, 188–204. (doi:10.1666/0094-8373(2001)027<0188:TIOPT>2.0.CO;2)
35. Jaeger J, Martinez-Arias A. 2009 Getting the measure of positional information. *PLoS Biol.* **7**, e1000081. (doi:10.1371/journal.pbio.1000081)

Fusco et al.

Electronic Supplementary Material

1. Supplementary figures

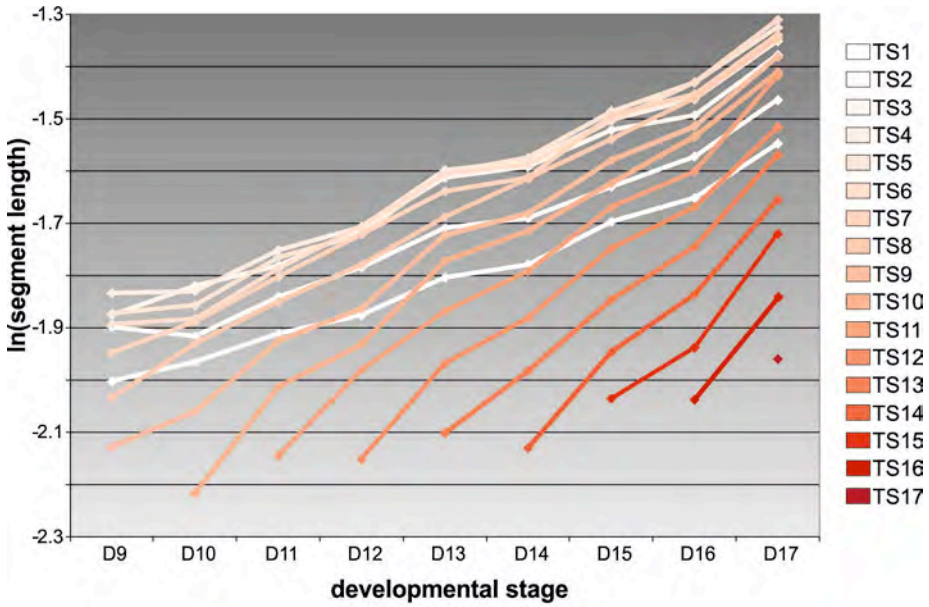

Figure S1. Observed log-transformed length of the thoracic segments during the meraspid stages D9-D17. Note the diverse average slopes of the different size progressions (see figure 2) and the crossing of the progression of some segments on those of the more anterior segments (e.g. TS10 and TS11 on TS1 and TS2). As a result of the differential average growth rate of the thoracic segments and the progressive schedule of their release into the thorax with a given initial size, during the meraspid ontogeny of *A. koninckii* there was a steady change in the relative size ranking of the thoracic segments, with the location of the longest segment moving progressively to the posterior, from being the 4th segment in stage D9 to the 6th segment in D17.

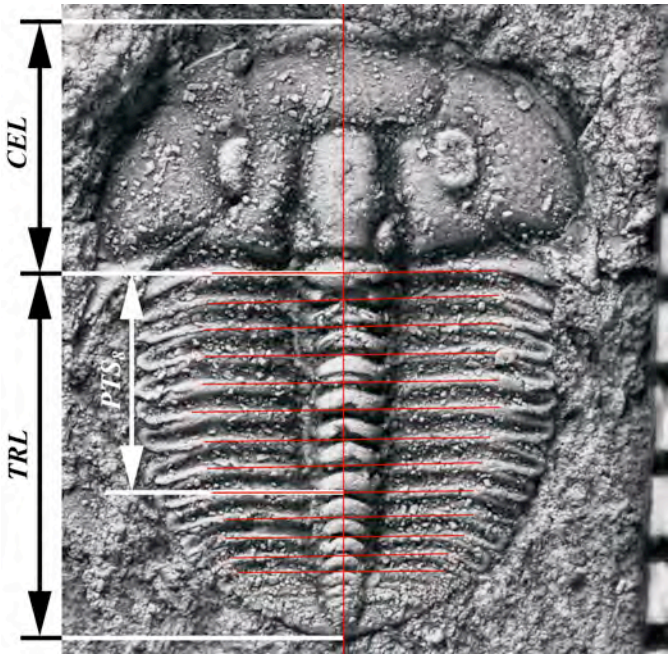

Figure S2. Measurements. A line along the sagittal axis was constructed on the image of each specimen and for each segment a line was then placed transversely to this, linking the articulating processes at the fulcral boss (the point abaxially marginal to the fulcrum). The intersections of these lines with the sagittal axis were used to calculate the length of each thoracic segment *i* (LTS_i) and the distance of the posterior boundary of thoracic segment *i* from cephalon/trunk boundary (PTS_i). PTS_8 is shown as an example. *CEL*: cephalic length; *TRL*: trunk length.

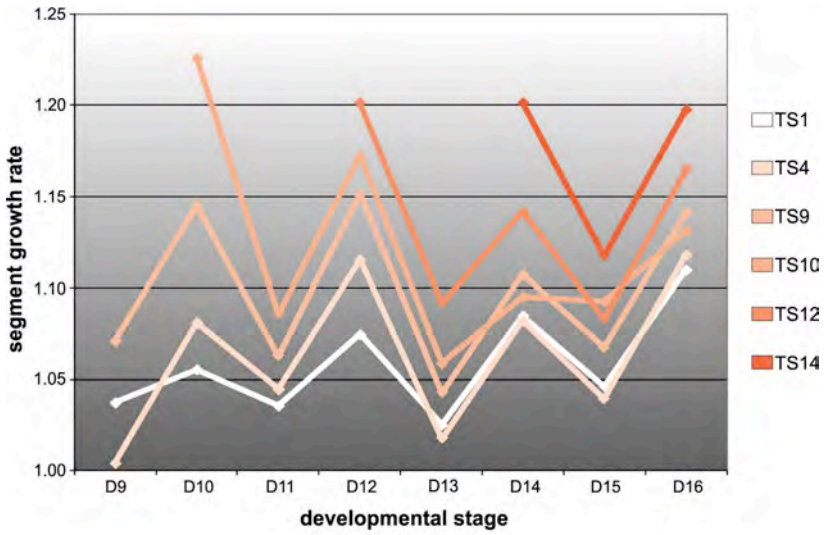

Figure S3. Observed per-stage growth rates of the length of a set of thoracic segments during the meraspid stages D9-D17. Distributions of values are very scattered because each value is the ratio between observed size values in two subsequent stages, which are extremely sensitive to sample errors. Note how all progressions fluctuate approximately in pace, due to the relatively underestimated average TS sizes in samples of D10, D12, D14, D16 with respect to samples of D9, D11, D13, D15, D17. This is the same residual pattern that emerges from the analysis of other size variables (see figure S6). The different expectations of different growth control models cannot be tested using this highly scattered dataset.

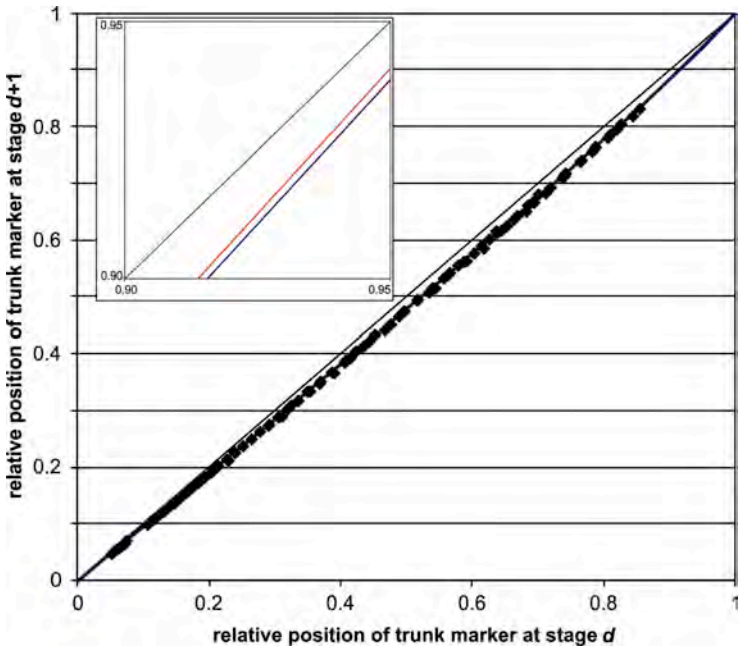

Figure S4. Fitting of the two *TG* models onto the change in relative trunk position for landmark points. Diamonds, observed distribution of $RPS_{i,d}$ vs. $RPS_{i,d+1}$, n=96; red line *TGexp* model; blue line *TGpwl* model. The predicted values of the two models are almost indistinguishable in the region of observed data (0.05-0.85), but are more divergent in the more posterior interval (see enlarged insert). The bisector of first quadrant (thin black line) is shown as a reference. Parameters values as in table S3 and figure S5.

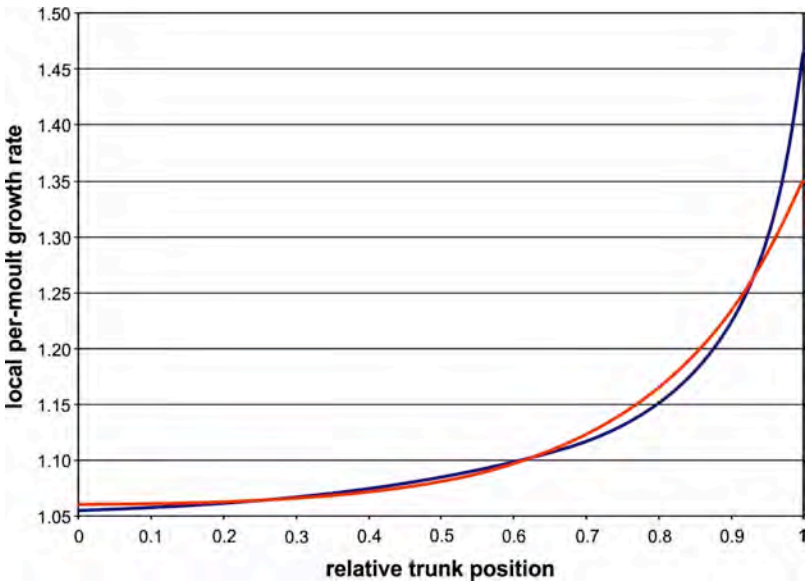

Figure S5. Growth gradients for the two *TG* models with the parameters estimated by fitting the change in relative trunk position for landmark points. Red line, *TGexp* model; blue line, *TGpwl* model. Parameters values as in table S3 and figure S4.

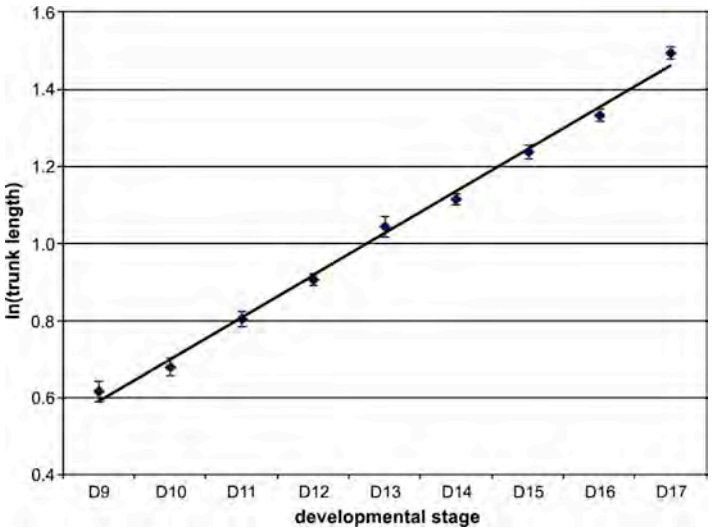

Figure S6. Ontogenetic size progression for the length of the trunk during the meraspid stages D9-D17. Least square linear regression of lnTRL_d on d (r^2=0.995, n=9). Bars are mean standard errors. In this section of ontogeny, trunk length conforms to a progression at a constant rate (Dyar's rule) [7,10]. The pattern of residuals also reflects the sampling error in calculating the averages of other size variables at different stages. This affects growth rate estimations (see figure S3).

2. Supplementary tables

Table S1. Results of AIC_c comparison onto $RLS_{i,d+1}$ dataset for the four competing models, taking out 4 outliers (observations with a studentized residual >3 for at least one of the models).

Model	*No. par.*	*RSS*	AIC_c	ΔAIC_c	$wAIC_c$
SGgmp	3	$1.74 \cdot 10^{-4}$	-1260.46	55.75	$5.09 \cdot 10^{-13}$
SGpwp	3	$1.72 \cdot 10^{-4}$	-1261.72	54.48	$9.58 \cdot 10^{-13}$
TGexp	2	$9.99 \cdot 10^{-5}$	-1316.20	0	0.649
TGpwl	3	$9.89 \cdot 10^{-5}$	-1314.97	1.23	0.351

No. par. = number of estimated parameters; *RSS* = residual sum of squares; AIC_c = corrected Akaike score; ΔAIC_c = difference in AIC_c score with respect to the model with the minimum score; $wAIC_c$ = Akaike weight, the probability of being the correct model among the set of candidate models. The strength of evidence in favour of one model (or a set of models) over a competing model (or a disjunct set of competing models), the evidential ratio, is the ratio between its Akaike weight (or the summation of the Akaike weights of the set of models) and the Akaike weight of the competing model (or the summation of the Akaike weights of the competing set). The evidential ratio of the two *TG* models vs. the two *SG* models is $6.82 \cdot 10^{11}$ and the evidential ratio of *TGexp* vs. *TGpwl* is 1.85. The number of observations ($RLS_{i,d}$) on which the calculation is based is 96.

Table S2. Results of AIC_c comparison onto $RLS_{i,d+1}$ dataset for the two *TG* competing models, taking out 4 outliers (observations with a studentized residual >3 for at least one of the models).

Model	*No. par.*	*RSS*	AIC_c	ΔAIC_c	$wAIC_c$	*R*
TGexp	2	$9.66 \cdot 10^{-5}$	-1319.45	0	0.615	1.599
TGpwl	3	$9.53 \cdot 10^{-5}$	-1318.51	0.94	0.385	

No. par. = number of estimated parameters; RSS = residual sum of squares; AIC_c = corrected Akaike score; ΔAIC_c = difference in AIC_c score with respect to the model with the minimum score; $wAIC_c$ = Akaike weight, the probability of being the correct model among the set of candidate models; *R* = evidential ratio. The strength of evidence in favour of one model over the competing model, the evidential ratio R, is the ratio of their Akaike weights. The number of observations ($RLS_{i,d}$) on which the calculation is based is 96.

Table S3. Results of AIC_c comparison onto $RPS_{i,d+1}$ dataset for the two *TG* competing models, taking out 4 outliers (observations with a studentized residual >3 for at least one of the models).

Model	*No. par.*	*RSS*	AIC_c	ΔAIC_c	$wAIC_c$	*R*
TGexp	2	$2.57 \cdot 10^{-4}$	-1225.44	2.78	0.199	
TGpwl	3	$2.44 \cdot 10^{-4}$	-1228.23	0	0.801	4.021

No. par. = number of estimated parameters; RSS = residual sum of squares; AIC_c = corrected Akaike score; ΔAIC_c = difference in AIC_c score with respect to the model with the minimum score; $wAIC_c$ = corrected Akaike weight, the probability of being the correct model among the set of candidate models; *R* = evidential ratio. The strength of evidence in favour of one model over the competing model, the evidential ratio R, is the ratio of their Akaike weights. The number of observations ($RPS_{i,d}$) on which the calculation is based is 96. Parameter values as in figures S4 and S5.

3. Measurements

The dataset used to explore growth progression of thoracic segments (TS) is based the ontogenetic interval of stages from D9 to D17 inclusive. This comprises 137 specimens. For each specimen (*s*), the following distance measurements were obtained from landmark coordinates (figure S2):

- *CEphalic Length* $CEL(s)$
- *TRunk Length* $TRL(s)$
- *Length of Thoracic Segment* i $LTS_i(s)$
- *Distance of the Posterior boundary of Thoracic Segment* i *from cephalon/trunk boundary* $PTS_i(s)$

For each thoracic segment *i* and developmental stage *d*, average measures were obtained from individual distance measures after transformation into their natural logarithms, a standard procedure in allometry analysis (E[] stands for arithmetic mean).

- *Average CEphalic Length* CEL_d=exp(E[ln($CEL(s)$)]) for all specimens *s* at stage *d*
- *Average TRunk Length* TRL_d=exp(E[ln($TRL(s)$)]) for all specimens *s* at stage *d*
- *Average Length of the Thoracic Segment* $LTS_{i,d}$=exp(E[ln($PTS_i(s)$)])-exp(E[ln($PTS_{i-1}(s)$)]) for all specimens *s* at stage *d*
- *Average Relative position of the Posterior boundary of the thoracic Segment* $RPS_{i,d}$=E[$PTS_i(s)/TRL(s)$] for all specimens *s* at stage *d*
- *Average Relative Length of the thoracic Segment* $RLS_{i,d}$=E[$LTS_i(s)/TRL(s)$] for all specimens *s* at stage *d*
- *Calculated average TRunk Length* $cTRL_d$ = antilogarithm of the corresponding estimated value from linear regression of lnTRL_d on *d* (see figure S6)

3. Fitting function derivation and fitting implementation

<u>*SGgmp* model</u>

The *SGgmp* model set the constant per-stage growth rate of each segment *i* as a geometric progression. The segmental gradient is a decaying geometric progression from the posterior of the thorax

(1) $g(i) = a + be^{wi}$

The *SGgmp* fitting function for the dataset of the relative size of thoracic segments is obtained as the product of the segment length at a given stage by its segment specific growth rate divided by the calculated trunk length at the following stage.

Dependent variable: $RLS_{i,d+1}$
Independent variables: $LTS_{i,d}$, i, $cTRL_d$
Fitting parameters: a, b, w
Fitting function: $RLS_{i,d+1} = LTS_{i,d}*(a+b*\exp(w*i))/cTRL_{d+1}$

<u>*SGpwp* model</u>

The *SGpwp* model set the constant per-stage growth rate of each segment *i* as a power progression. The segmental gradient is a decaying power progression from the posterior of the thorax

(1) $g(i) = a + bi^{w}$

The *SGpwp* fitting function for the dataset of the relative size of thoracic segments is obtained as the product of the segment length at a given stage by its segment specific growth rate divided by the calculated trunk length at the following stage.

Dependent variable: $RLS_{i,d+1}$
Independent variables: $LTS_{i,d}$, i, $cTRL_d$
Fitting parameters: a, b, w
Fitting function: $RLS_{i,d+1} = LTS_{i,d}*(a+b*i\text{^}w)/cTRL_{d+1}$

TGexp model

The *TGexp* model set the local per-stage growth rate at each point along the trunk as an exponential function. For any point x in the closed interval [0,1] of relative anterior-posterior trunk positions, the growth gradient is a decaying exponential function from the posterior

(1) $g(x) = a + be^{-w(1-x)}$

and the average growth of the section of the trunk until position x [0,x] is

(2) $$G(x) = \frac{\int_0^x g(y)dy}{x-0} = a + \frac{-be^{-w} + be^{-w(1-x)}}{wx}$$

In order for the average growth rate of the whole trunk to be equal to the observed average rate (r), we set $G(1)=r$ and solving (2) for a with this constraint gives

(3) $$a = \frac{b(-1+e^{-w}) + rw}{w}$$

Substituting (3) into (1), the gradient function reduces to two parameters

(4) $$g(x) = \frac{b(-1+e^{-w}) + rw}{w} + be^{-w(1-x)}$$

and substituting (3) into (2), the integral function reduces to two parameters

(5) $$G(x) = r + \frac{-be^{-w} + be^{-w(1-x)} + bx(-1+e^{-w})}{wx}$$

Dividing (5) by r (to scale to relative growth) and multiplying by x (the current relative position of a given landmark) we get

(6) $$Z(x) = x + \frac{-be^{-w} + be^{-w(1-x)} + bx(-1+e^{-w})}{rw}$$

For a landmark at position x along the trunk at a given stage, $Z(x)$ is the relative position of the same landmark at the following stage.

Fitting of the relative length of thoracic segments ($RLS_{i,d+1}$)

The fitting function is the difference between the positions of two landmarks: the posterior and the anterior boundaries of each segment. The position of the anterior boundary of a given segment coincides with that of the posterior boundary of the preceding segment or, for the first thoracic segment, with the most anterior trunk landmark (x=0).

Dependent variable: $RLS_{i,d+1}$
Independent variable: $RPS_{i,d}$
Fitting parameters: b, w
Fixed parameter: r = 1.11528
Fitting function: $RLS_{i,d+1} = Z(RPS_{i,d})\text{-}Z(RPS_{i\text{-}1,d})$

Fitting of the relative position of the posterior boundary of thoracic segments ($RPS_{i,d+1}$)

Dependent variable: $RPS_{i,d+1}$
Independent variable: $RPS_{i,d}$
Fitting parameters: b, w
Fixed parameter: r = 1.11528

Fitting function: $RPS_{i,d+1} = Z(RPS_{i,d})$

TGpwl model

The *TGpwl* model set the local per-stage growth rate at each point along the trunk as a power law function. For any point x in the close interval [0,1] of relative anterior-posterior trunk positions, the growth gradient is a decaying power law function from posterior

(1) $g(x) = a + b(1 - x + c)^{-w}$

and the average growth of the section of the trunk until position x [0,x] is

(2) $G(x) = \dfrac{\int_0^x g(y)dy}{x - 0} = a + \dfrac{b(1+c)^{1-w} - b(1+c-x)^{1-w}}{x(1-w)}$

In order for the average growth rate of the whole trunk to be equal to the observed average rate (r), we set $G(1)=r$ and solving (2) for a with this constraint gives

(3) $a = r + \dfrac{bc^{1-w} - b(1+c)^{1-w}}{1-w}$

Substituting (3) into (1), the gradient function reduces to two parameters

(4) $g(x) = r + \dfrac{bc^{1-w} - b(1+c)^{1-w}}{1-w} + b(1-x+c)^{-w}$

and substituting (3) into (2), the integral function reduces to two parameters

(5) $G(x) = r + \dfrac{b(-(1+c-x)^{1-w} + (1-x)(1+c)^{1-w} + xc^{1-w})}{x(1-w)}$

Dividing (5) by r (to scale to relative growth) and multiplying by x (the current relative position of a given landmark) we finally get

(6) $Z(x) = x + \dfrac{b(-(1+c-x)^{1-w} + (1-x)(1+c)^{1-w} + xc^{1-w})}{r(1-w)}$

For a landmark at position x along the trunk at a given stage, $Z(x)$ is the relative position of the same landmark at the following stage.

Fitting of the relative length of thoracic segments ($RLS_{i,d+1}$)

The fitting function is the difference between the positions of two landmarks: the posterior and the anterior boundaries of each segment. The position of the anterior boundary of a given segment coincides with that of the posterior boundary of the preceding segment or, for the first thoracic segment, with the most anterior trunk landmark (x=0).

Dependent variable: $RLS_{i,d+1}$
Independent variable: $RPS_{i,d}$
Fitting parameters: b, c, w
Fixed parameter: r = 1.11528
Fitting function: $RLS_{i,d+1} = Z(RPS_{i,d}) - Z(RPS_{i-1,d})$

Fitting of the relative position of the posterior boundary of thoracic segments ($RPS_{i,d+1}$)

Dependent variable: $RPS_{i,d+1}$
Independent variable: $RPS_{i,d}$
Fitting parameters: b, c, w
Fixed parameter: r = 1.11528
Fitting function: $RPS_{i,d+1} = Z(RPS_{i,d})$